Online EIS Measurement Method for Lithium-Ion Battery Energy Storage Systems

1st Fu Li
Institute of Electrical Engineering, CAS
University of Chinese Academy of Sciences
Beijing, China
lfxwj@mail.iee.ac.cn

2nd Xisheng Tang*
Institute of Electrical Engineering, CAS
University of Chinese Academy of Sciences
Key Laboratory of Long-Duration and Large-Scale Energy Storage
Beijing, China
tang@mail.iee.ac.cn

3rd Shuang Song
Institute of Electrical Engineering Chinese Academy of Sciences
Key Laboratory of Long-Duration and Large-Scale Energy Storage
Beijing, China
songshuangiee@mail.iee.ac.cn

4th Yushu Sun
Institute of Electrical Engineering Chinese Academy of Sciences
Beijing, China
yushusun@mail.iee.ac.cn

5th Yanglin Zhou
State Key Laboratory of Power System Operation and Control
Tsinghua University
Beijing, China
zhouylstu@tsinghua.edu.cn

6th Song Ci
Department of Electrical Engineering
State Key Laboratory of Power System Operation and Control
Tsinghua University
Beijing, China
sci@tsinghua.edu.cn

7th Chengjie Zhang
Huadian Inner Mongolia Energy Co., Ltd
Hohhot, China
chengjie-zhang@chd.com.cn

***Abstract*—Online battery impedance identification is an effective tool for evaluating the electrochemical state and ensuring safe operation of energy storage systems. Conventional EIS methods are costly, time-consuming, and limited to offline low-voltage tests. This paper proposes an inverter-based online impedance identification method that achieves broadband measurement without additional excitation circuits. By modulating the AC-side current amplitude, controllable perturbations are introduced on the DC side, enabling clear correlation between the injected and response signals for accurate EIS acquisition. A battery–SiC inverter–three-phase platform was built to validate the approach. Experiments on 302 Ah cells demonstrate that broadband impedance from 0.1 Hz to 100 Hz can be identified within 21 s, with results consistent with those of conventional electrochemical workstations. The proposed method eliminates voltage limitations, greatly shortens measurement time, and provides a low-cost and high-efficiency solution for real-time impedance monitoring of high-capacity batteries.**

***Index Terms*—electrochemical impedance spectroscopy, inverter, binary sequence signal, energy storage.**

I. Introduction

Electrochemical energy storage systems are indispensable for modern power and transportation infrastructures, driven by the growth of renewable energy integration and electrified mobility [1]. Understanding and maintaining battery health is thus essential for ensuring long-term reliability and safety [2]. Electrochemical impedance spectroscopy (EIS) is a powerful diagnostic and modeling tool [3], as the impedance spectrum reflects electrochemical parameters such as state of charge (SOC), state of health (SOH), temperature, and degradation mechanisms. Through impedance modeling, charge transfer, diffusion, and interfacial kinetics can be characterized quantitatively, supporting battery state estimation and aging analysis.

Despite its laboratory success, online implementation of EIS remains challenging. Conventional methods require external excitation, precise instrumentation, and long acquisition time, limiting practical deployment. To overcome this, recent studies focus on embedding impedance measurement within existing power electronic interfaces [4], which can be categorized by whether additional excitation circuits are required.

The first category employs dedicated excitation sources such as pseudorandom sequences, broadband multisines, or digitally synthesized perturbations. Yao et al. [5] developed an online EIS technique by inserting a small SRC circuit into the converter. The second category eliminates extra hardware by utilizing inherent converter switching behavior or control freedoms. BMS-, DC/DC-, and DC/AC-based techniques achieve online EIS through signal modulation and current reconstruction. Liu et al. [6] proposed a dual-frequency MMB architecture enabling both EIS and self-heating.

Although not originally intended for EIS, battery-connected converters can embed online impedance functions. Nonisolated DC/DC converters are most common for their simplicity. Geng et al. [3] introduced a broadband EIS scheme using a bidirectional converter with DIBS excitation, while Assadi et al. [7] implemented a GaN-based triple-active bridge converter

979-8-3315-8138-1

for variable-frequency EIS perturbation.

In inverter-based EIS, Howey et al. [8] used motor controller–generated excitation from 1 Hz to 2 kHz, though the perturbation was uneven across frequencies. Qu et al. [9] achieved broadband inverter-based impedance identification without external excitation via controllable AC perturbations.

Most studies remain confined to DC/DC topologies, as inverter-based implementations face complex AC/DC coupling and spectral control challenges. This paper proposes an AC/DC converter–based online impedance measurement method that modulates AC-side current amplitude using a multi-frequency binary sequence, generating broadband DC-side perturbations without added hardware. The approach enables rapid impedance acquisition with minimal system disturbance, offering a practical solution for integrating EIS functionality into power conditioning systems (PCS) for continuous in-situ monitoring of large-scale energy storage systems.

The paper is organized as follows: Section II details the proposed method; Sections III and IV present simulation and experimental results; Section V concludes the work.

II. Online EIS Measurement Method

The Nyquist plot of the LFP cell measured offline using an electrochemical workstation is shown in Fig. 1. It can be divided into three regions: high-, mid-, and low-frequency. The high-frequency region reflects electron and ionic conduction processes, while the mid-frequency region corresponds to charge transfer and ionic migration through SEI and CEI films. The low-frequency region represents solid-phase diffusion within the electrode. The frequency where the imaginary impedance equals zero is defined as f_0, and the turning point between mid- and low-frequency regions is f_{tr}. For LFP cells, f_0 is typically 100–60 Hz and f_{tr} 2–0.5 Hz, whereas for NCM cells, f_0 is about 200 Hz and f_{tr} around 2 Hz. The mid-frequency region is closely related to SOC, SOH, and lithium plating behavior. Considering the sampling rate limit (below kHz) in practical systems, the frequency range in this study is set to 100–0.1 Hz, covering the entire mid-frequency band and part of the low-frequency band.

A. Small-Current Excitation Injection Method

The online EIS measurement architecture is shown in Fig. 2, consisting of a series-connected battery string, an AC/DC converter, a DC-side capacitor, and an AC-side inductor. The AC side is connected to the grid. The signals acquired for EIS measurement are the current flowing through the battery and the corresponding voltage. Therefore, this approach is not limited to series-connected strings and is also applicable to parallel multi-string configurations.

The proposed online EIS method is based on the law of energy conservation between the AC and DC sides. A small, uniform AC signal is injected through inverter control, causing power fluctuations at the excitation and fundamental frequencies. These fluctuations couple to the DC side, eliciting the battery's response signal necessary for impedance identification [9].

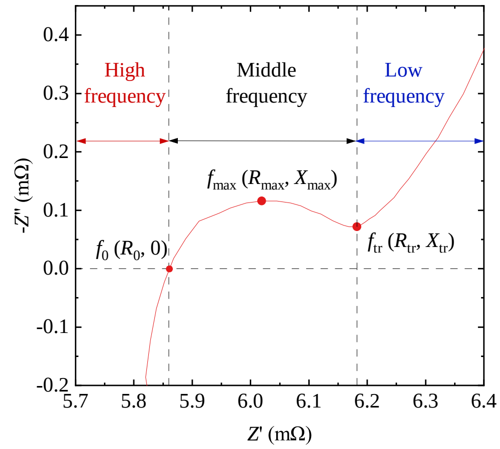

Fig. 1. Offline EIS Nyquist plot of the LFP cell.

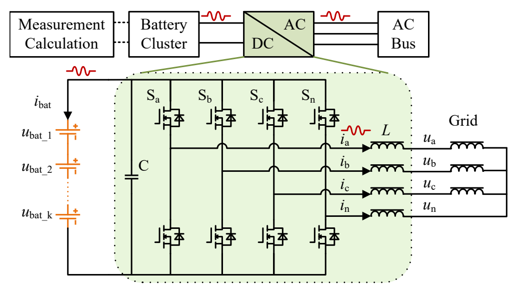

Fig. 2. Schematic diagram of the online EIS measurement.

Assuming three-phase balance ($i_n = 0$), the d–q transformation separates the fundamental and injected frequencies, allowing a sinusoidal DC-side current under high switching frequency. However, low switching frequency limits the measurable range. To address this, a multi-frequency binary excitation is employed to reduce converter dynamic constraints, broaden the measurable EIS bandwidth, and shorten total measurement time.

For the measurement framework shown in Fig. 1, the AC-side current and voltage are expressed in (1) and (2), assuming an AC-side power factor of 1.

$$\begin{bmatrix} i_a \\ i_b \\ i_c \end{bmatrix} = A_e \mathrm{sgn}(\sin(\omega_e t)) \begin{bmatrix} \sin(\omega_o t) \\ \sin(\omega_o t - 2/3\pi) \\ \sin(\omega_o t + 2/3\pi) \end{bmatrix} \tag{1}$$

$$\begin{bmatrix} u_a \\ u_b \\ u_c \end{bmatrix} = A_u \begin{bmatrix} \sin(\omega_o t) \\ \sin(\omega_o t - 2/3\pi) \\ \sin(\omega_o t + 2/3\pi) \end{bmatrix} \tag{2}$$

Where, A_e denotes the AC-side current amplitude, ω_e is the frequency of current amplitude variation, and ω_0 is the AC-side fundamental frequency. The phase-A power is given by (3).

979-8-3315-8138-1

$$
\begin{aligned}
P_a &= i_a(L\frac{di_a}{dt}+u_a) \\
&= L\omega_o {A_e}^2 \mathrm{sgn}^2(\sin(\omega_e t))\sin(\omega_o t)\cos(\omega_o t) \\
&+A_e\frac{d\mathrm{sgn}(\sin(\omega_e t))}{dt}\sin(\omega_o t) \\
&+A_e A_u \mathrm{sgn}(\sin(\omega_e t))\sin^2(\omega_o t)
\end{aligned} \tag{3}
$$

Neglecting line losses but considering converter losses, the AC-side power equals the power flowing through the battery, as expressed in (4).

$$
(u_{bat}+\tilde{u}_{bat})(i_{bat}+\tilde{i}_{bat})+P_{cap}=\frac{3}{2}A_u A_e \mathrm{sgn}(\sin(\omega_e t))+P_{loss} \tag{4}
$$

Where, u_{bat} and $\tilde{u}_{bat}$ represent the DC and AC components of the cell voltage, respectively; i_{bat} and $\tilde{i}_{bat}$ are the DC and AC components of the cell current; P_{cop} denotes the power through the battery; and P_{loss} represents the AC/DC converter loss.

According to (4), when the AC-side current amplitude varies at ω_e, the DC-side current generates a corresponding same-frequency current excitation injected into the battery. By selecting a sufficiently small A_e, the DC side produces a small-signal current excitation, inducing low-amplitude voltage fluctuations (¡10 mV) in the cell, which allows measurement of the battery impedance at the frequency ω_e.

B. Multi-Frequency Excitation Signal

A multi-frequency superimposed square-wave excitation is constructed for the AC-side current amplitude A_e based on first principles, maximizing the energy contribution at the target frequencies. The superposition of the specified-frequency sinusoidal signals is given in (5).

$$
S(t)=\sum_{i=1}^{N_{\mathrm{freq}}} A_i \sin(2\pi f_i \cdot t+\varphi_i) \tag{5}
$$

Where, t denotes the time of the excitation signal; S is the superposition of all sinusoidal signals; N_{freq} is the total number of frequencies in the impedance spectrum; i is the index of the impedance frequency; f_i is the i-th impedance frequency; A_i is the amplitude at the i-th frequency; and ϕ_i is the phase angle at the i-th frequency.

The square-wave excitation Q(t) is constructed based on S(t).

$$
Q(t)=\begin{cases} B, \mathrm{S(t)}>0 \\ -B, \mathrm{S(t)}<0 \\ B \mathrm{or} -B, \mathrm{S(t)}=0 \end{cases} \tag{6}
$$

Where, Q denotes the square-wave excitation, and B is its amplitude.

The generated Q(t) is subjected to an FFT, and the resulting phase angles are updated in ϕ_i of (5). This process is iterated until the phase angles converge [3]. The final excitation sequence for the AC-side current amplitude A_e is thus obtained. For a measurement frequency range of 100 Hz–0.1 Hz, the sequence duration is set to 20 s.

TABLE I
FIRST-ORDER RC EQUIVALENT CIRCUIT.

Parameter	V_{oc}(V)	R_0(mΩ)	R_1(mΩ)	C_1(F)
Value	3.25	0.242	0.909	30

The date acquisition and processing part contains seven steps. 1) Sample the current and voltage data of the battery system with online EIS function at a fixed frequency f_s. 2) Perform antialiasing filtering of the sampling data using a digital filter. 3) Valid data extraction. The aim is to exclude transient data and form new n data segments. 6) Conduct FFT on n data segments to generate battery voltage and current components at n target frequencies. 7) Calculate and plot EIS. Other battery impedance characteristics will be analyzed also if necessary. The impedance is calculated as shown in (7).

$$
Z(f_i)=\frac{U(f_i)\angle\varphi_{U_{fi}}}{I(f_i)\angle\varphi_{I_{fi}}} \tag{7}
$$

Where, $Z(f_i)$ is the impedance at frequency f_i; $U(f_i)$ and $\varphi_{U_{fi}}$ are the voltage amplitude and phase angle at f_i, respectively; and $I(f_i)$ and $\varphi_{I_{fi}}$ are the current amplitude and phase angle at f_i, respectively.

III. SIMULATION RESULTS AND ANALYSIS

A simulation model for online EIS characterization is established as shown in Fig. 2. The battery is represented by a first-order RC equivalent circuit to capture charge transfer impedance characteristics, with parameters listed in Table I. R_0 denotes the total ohmic resistance of the electrolyte, current collector, active material, and separator, influenced by cell structure and electrode properties. The RC branch represents the double-layer capacitance C_1 and charge transfer resistance R_1, where electron movement across the electrolyte–collector interface causes R_1 and the resulting interfacial polarization forms C_1.

The simulation parameters of the online EIS measurement model are listed in Table II. During the simulation, the target impedance frequencies range from 0.1 Hz to 100 Hz. The switching frequency is set to 40 kHz, and the sampling frequency is 1 kHz to closely replicate the BMS sampling rate in practical scenarios. The AC-side current amplitude Ae is set to 13.9 A to ensure that the battery voltage response remains around ±10 mV. The AC-phase voltage RMS value is 220 V, and the DC-side battery string consists of 200 series-connected cells, each with a nominal voltage of 3.25 V, resulting in a total DC voltage of 650 V. The excitation sequence is applied by controlling the d-axis component of the AC-side current. The time-domain and frequency-domain waveforms of the battery-side current at the AC/DC converter are shown in Figs. 3.

The simulated EIS measurement results for different excitation methods are shown in Fig. 4. The reference values are calculated from the impedance of the equivalent circuit at different frequencies. The figure compares the measurements obtained using multi-sine excitation, binary excitation under 0 A charging current. In summary, the multi-sine excitation

TABLE II
SIMULATION MODEL PARAMETERS.

Symbol	Parameter	Value
C	DC-side capacitor	1880uF
L	AC-side inductor	200uH
f_t	Target frequency	100-0.1Hz
f_o	Fundamental frequency	50Hz
A_e	Excitation current amplitude	13.9A
f_s	Sampling frequency	1kHz
f_sw	Switching frequency	40kHz

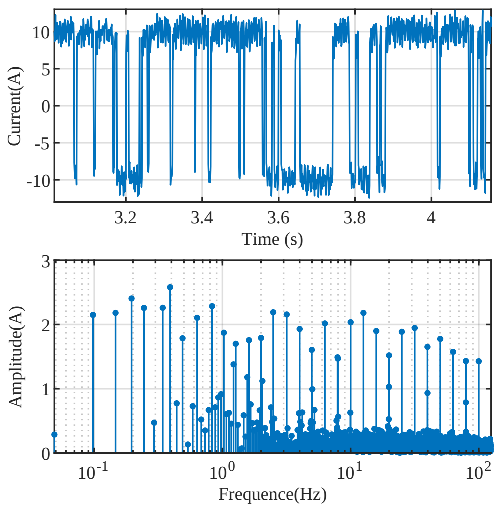

Fig. 3. Time-domain and frequency-domain waveforms of the battery current.

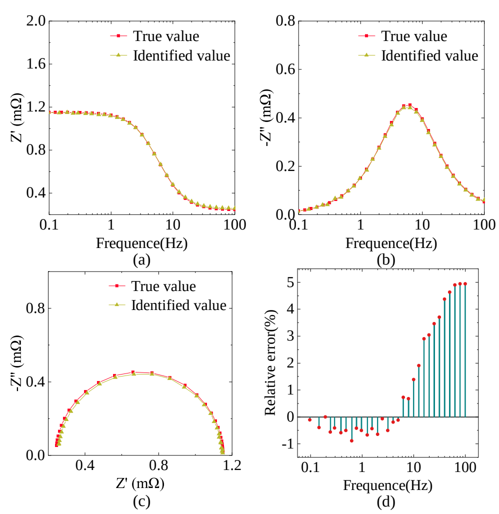

Fig. 4. EIS results of the online AC/DC converter compared with true values. (a) Frequency response of the real part of impedance; (b) Frequency response of the imaginary part of impedance; (c) Nyquist plot of EIS; (d) Relative error.

method produces fewer harmonic components and higher accuracy but requires segmented spectral analysis and longer sweep times. The binary excitation method inherently contains harmonic components, does not require frequency sweeping, and shortens the measurement time at the expense of accuracy. Therefore, a trade-off between EIS accuracy and measurement time must be considered when designing an excitation suitable for energy storage battery EIS measurement and lithium plating detection.

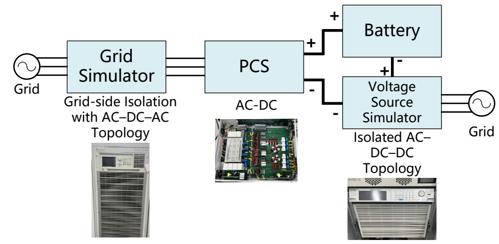

Fig. 5. Experimental platform for online EIS characterization.

IV. EXPERIMENTAL VALIDATION

To verify the proposed online EIS characterization method, an experimental platform was constructed, as shown in Fig. 5. A 302Ah LFP cell designed for energy storage was selected, with parameters listed in Table IV. The programmable dc power supply, serially connected to the battery, boosts and stabilizes dc bus voltage while maintaining a constant battery discharge rate under a fixed load. It also limits current to prevent excessive discharge, enhancing experimental safety. In fact, it is feasible to use more series-connected battery modules instead of a dc power source to meet the voltage level on the dc side. Nevertheless, this approach has not been adopted due to concerns over experimental safety.

A conventional three-phase, four-leg topology was chosen for the AC/DC converter. The switching devices are Wolfspeed C3M0040120K SiC MOSFETs, supporting a switching frequency of 40 kHz. The control core board is a TMS320F28335 DSP, responsible for signal control and PWM signal output.

The tests were conducted at 25 °C. The experimental waveforms are shown in Fig. 6. The relaxation time during the test was 20.48s, and the cell voltage fluctuation remained within 15mV, satisfying the ± 10 mV requirement. The temperature and voltage were consistent before and after the test. The frequency-domain characteristics of the battery current and voltage signals, obtained via FFT, are shown in Fig.7. At low frequencies, the amplitudes of current and voltage are relatively high, while at high frequencies, the amplitudes decrease. This phenomenon is due to the converter's stepwise current transitions, which are limited by its dynamic response, causing attenuation of high-frequency signals. However, the amplitudes at the target high-frequency points remain higher than those of adjacent frequencies, ensuring that EIS measurement is still feasible.

The Nyquist plot of the EIS is shown in Fig. 8. The EIS results were validated using the Kramers-Kronig test, yielding a chi-squared value of 7.91×10^{-6}, satisfying the criteria for stability, linearity, and causality. Compared with offline measurements from an electrochemical workstation, the overall trends are consistent. It is noteworthy that the semicircle in the online measurement is slightly smaller than that of the offline measurement, with a deviation of approximately $0.03\text{m}\Omega$. This

979-8-3315-8138-1

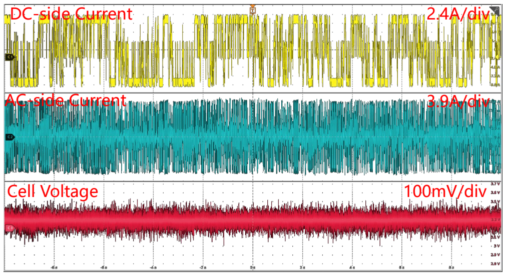

Fig. 6. Experimental waveforms corresponding to the DC-side current, AC-side current, and DC-side voltage.

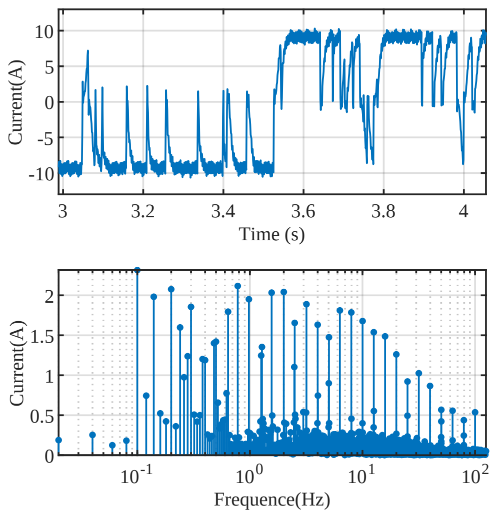

Fig. 7. Frequency-domain distribution of the battery current

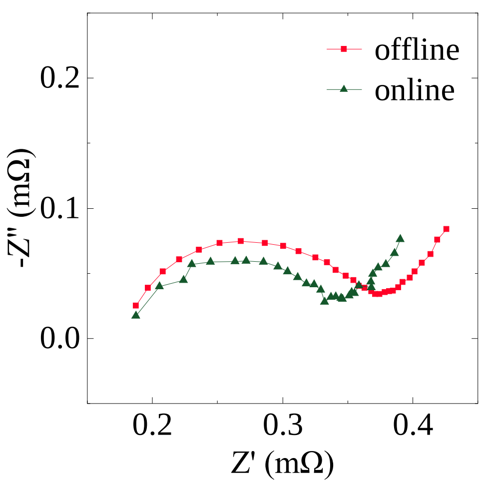

Fig. 8. Nyquist plot of the experimentally measured EIS.

discrepancy arises from multiple factors. The battery is a complex nonlinear system, and the current injected during online testing differs from that used in offline testing, causing subtle differences in the electrochemical kinetics. Additionally, differences in the signal-to-noise ratio of the excitation, sensor errors, and analog-to-digital conversion during online testing contribute to this deviation. The focus of this article is not to understand the mechanism of battery reaction but to design a low-cost and high availability battery condition monitoring means.

V. Conclusion

This paper presents an innovative online battery impedance identification method based on a battery-connected inverter. By modulating AC-side current to generate controllable DC-side perturbations, the approach enables broadband EIS measurement without additional excitation circuits and clarifies the underlying identification mechanism. An experimental platform comprising a battery, SiC inverter, and three-phase load was developed. Tests on 302 Ah cells verified the method's effectiveness, completing broadband impedance identification (0.1–100 Hz) within 21 s. Compared with conventional electrochemical workstations, this approach removes voltage limitations and significantly reduces measurement time.

Acknowledgment

This work was financially supported by a grant from the National Key Research and Development Program of China (No. 2023YFB2407902), Youth Innovation Promotion Association of Chinese Academy of Sciences (No. 2023000018), China Huadian Corporation Technology Program (No. CHT-GF-FW-2024-020), and autonomous research project of Key Laboratory of Long-Duration and Large-Scale Energy Storage (KLLLES) (No.2025ZD-06).

References

[1] S. Zhou, W. Du, B. Mager, P. R. Shearing, T. S. Miller, and R. Jervis, "Batch diagnosis of batteries within one second," Joule, 2025.

[2] H. Liu, et al., "Multi-modal framework for battery state of health evaluation using open-source electric vehicle data," Nat. Commun., vol. 16, no. 1, Art. no. 1, Jan. 2025.

[3] A. Geng, H. Hu, Y. Peng, Z. Zhao, Z. He, and S. Gao, "Wideband measurement approach for EIS of lithium-ion batteries using low-frequency concentrated disturbance," IEEE Trans. Ind. Electron., vol. 71, no. 5, pp. 4851–4860, May 2024.

[4] M. Bai, et al., "Converter-Based Online Battery Impedance Spectrum Measurement Using a Random Low-Frequency-Modulated Multisine Excitation," IEEE Trans. Transp. Electrif., vol. 11, no. 2, pp. 6763–6774, Apr. 2025.

[5] Q. Yao, D.-D.-C. Lu, and G. Lei, "Accurate Online Battery Impedance Measurement Method with Low Output Voltage Ripples on Power Converters," Energies, vol. 14, no. 4, Feb. 2021.

[6] M. Liu, Y. Chen, Y. Elasser, and M. Chen, "Dual Frequency Hierarchical Modular Multilayer Battery Balancer Architecture," IEEE Trans. Power Electron., vol. 36, no. 3, pp. 3099–3110, Mar. 2021.

[7] S. A. Assadi, et al., "In-Situ EV Battery Electrochemical Impedance Spectroscopy with Pack-Level Current Perturbation from a 400V-to-12V Triple-Active-Bridge," in 2022 IEEE Applied Power Electronics Conference and Exposition (APEC), Mar. 2022, pp. 1056–1063.

[8] D. A. Howey, P. D. Mitcheson, V. Yufit, G. J. Offer, and N. P. Brandon, "Online Measurement of Battery Impedance Using Motor Controller Excitation," IEEE Trans. Veh. Technol., vol. 63, no. 6, pp. 2557–2566, Jul. 2014.

[9] H. Qu, D. Luo, D. Jiang, M. Zhou, X. Zhao, and W. Sun, "Online Battery Impedance Identification Based on Small AC Signal Injection of Inverter," IEEE Trans. Power Electron., vol. 40, no. 2, pp. 3490–3504, Feb. 2025.

979-8-3315-8138-1